

AI-Enhanced UAV Framework for Comprehensive Forest Fire Control and Ecosystem Recovery

Fathima Fida P¹, N S Parvathy², Glenn George K R³, Girish P⁴,
Muhammed Yazeen C Y⁵

^{1,2,3,5}Robotics and Automation, Toc H Institute of Science and Technology Ernakulam, Kerala, India

⁴Assistant Professor, Robotics and Automation, Toc H Institute of Science and Technology Ernakulam, Kerala, India

Abstract

This paper reports on the development and deployment of an autonomous UAV system for detecting, managing and post-fire replanting. The proposed system contains UAV using AI with advanced fire detection and reporting capabilities. Also comprises innovative firefighting and seed dispersal mechanisms for fire suppression and ecological recovery. First, it uses forest fire detection based on AI algorithms that analyze data from onboard sensors to identify early-stage fires. It then applies IoT technology to relay precise fire locations to emergency response teams in real time. SolidWorks was used to carry out structural design and fabrication, using extruded aluminum as the primary material. Using the Python-based program, it has navigation and suppression systems that guide the UAV to fire zones without any interference. It drops its payload with great precision in order to extinguish fires and has a fireball dispersal mechanism to disperse embers upon putting out the fire. The system has a replanting mechanism to restart ecological regeneration after suppressing fires by spreading seeds. This is to maximize fire management effectiveness and achieve environmental sustainability.

Keywords: Autonomous UAV, forest fire management, fire suppression, AI algorithms, IoT, seed dispersal, reforestation, trajectory optimization.

INTRODUCTION

The use of autonomous UAVs in the management of forest fires is a new advancement toward environmental catastrophe response and ecosystem restoration. These UAVs put to use the latest technology in fire detection through AI systems, IoT-based real-time data sharing, and precision navigation to quickly respond to natural disasters such as forest fires. These devices allow authorities to respond and take effective action immediately by quickly identifying fire signs that could lead to d in natural catastrophes, thus damaging[1], [6].

UAVs With seed ball distribution, UAVs also make a great contribution to environmental rejuvenation by automating the process of reforestation. This scalable approach improves ecosystem recovery through proper restoration of soils and the eradication of deforestation. Additionally, advanced mapping capabilities provide accurate land assessments, which are used to inform conservation and targeted efforts

[2], [3].

It includes biodiversity monitoring, sustainable land restoration, climate research, and so forth, in its scope outside of fire management. With AI, IoT, and advanced robotics, UAV systems open up avenues for proactive disaster management as well as sustainable environmental preservation with a new leap in strategies of environmental conservation [9], [10].

SYSTEM MODEL

The proposed autonomous UAV system enhances forest fire management by the application of different strategies. High-performance AI algorithms differentiate flames from natural heat sources through visual data processing for the early detection of fire. Aluminum lightweight framing ensures the ruggedness of UAVs, whereas the navigation system based on Python is combined with GPS and inertial guidance, allowing precise autonomous flight.

Real-time IoT communication transmits data to emergency response teams to take appropriate action. Precision fireball dispersion mechanisms target effective fire suppression. GPS-guided seed ball dispersal post-fire promotes reforestation. This methodology is an integration that provides for efficient detection, suppression of fire, and recovery of ecosystems in support of environmental protection and safety for the community.

System Design

This The quadcopter control system, as illustrated in Figure 1, is designed with a SpeedyBee V3 flight controller as the central processing unit, responsible for managing flight stability, navigation, and telemetry communication. The system is powered by a 14.8V 5200mAh LiPo battery, which supplies energy to the flight controller, 4-in-1 ESC (Electronic Speed Controller), and additional peripherals. For navigation, a Neon M8N GPS module provides real-time positioning, while 3DR telemetry modules enable wireless communication with the ground station. A Raspberry Pi, connected to a camera module, enhances onboard processing and vision-based tasks.

Additionally, the system features a gripper mechanism, controlled by the flight controller for object handling. The power distribution system efficiently supplies power and facilitates data communication between all components.

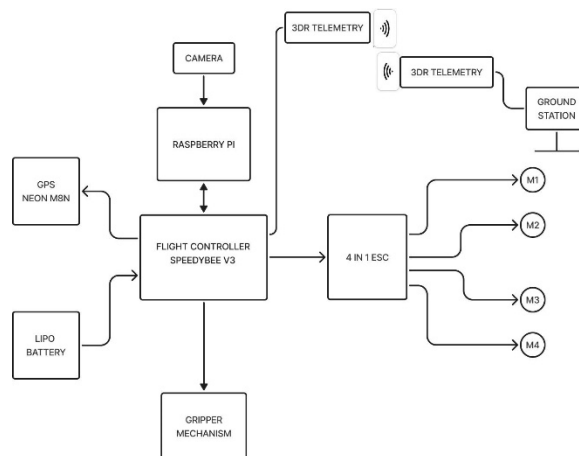


Figure 1 : Block Diagram of the Hardware System

The design prioritizes safety through redundant connections and failsafe protocols while maintaining efficient power management and minimal latency in control operations.

Mechanical Design

The structural design of the quadcopter was developed in SolidWorks as illustrated in the isometric view with dimensions in Figure 2. The frame is constructed using an aluminum alloy, chosen for its high strength-to-weight ratio, ensuring a lightweight yet robust framework and flexible PLA for the gripper for precision handling and adaptability during payload operations., ensuring a balance between weight reduction and durability under operational stresses.

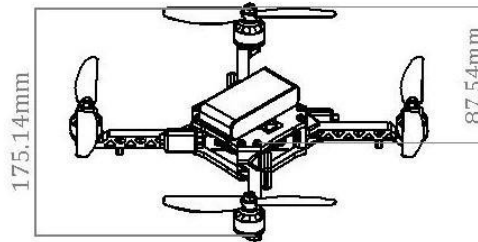


Figure 2 : Isometric view of the drone

Optimized Load Distribution

The quadcopter design ensures uniform load distribution to maintain structural integrity and enhance flight stability. The following weight distribution analysis highlights the contributions of various components:

Table 1: Load Distribution

Component	Weight (kg)
Frame	0.4
Motors (4x60g)	0.24
ESC	0.1
Battery	0.45
Propellers (4x10g)	0.04
Raspberry Pi	0.05
Servomotor	0.03
Other Electronics	0.1
Payload (including dropping mechanism)	0.3
Total Weight	1.3

This optimized load distribution ensures that the quadcopter maintains a center of gravity conducive to stable flight, even under payload conditions.

Modular Assembly

The modular design of the quadcopter simplifies maintenance and upgrades by allowing independent replacement of components such as the gripper and electronics, thereby minimizing downtime and enabling future feature integration. The use of lightweight extruded aluminum and flexible PLA ensures durability and adaptability across various operational scenarios. Balanced weight distribution across the

quadcopter frame enhances flight stability, preventing localized stresses and ensuring consistent performance during flight. The isometric design, as shown in Figure 2, provides a clear representation of the structural components and dimensions, highlighting the efficiency of the overall design.

Power Requirements

The power requirements for the UAV are designed to ensure efficient operation under the specified load conditions.

Each motor consumes 88.8 W, calculated as:

$$\text{Power per Motor} = 6\text{A} \times 14.8\text{V} = 88.8\text{W} \quad (1)$$

With four motors, the total power consumption for propulsion is:

$$\text{Total Power Consumption} = 88.8\text{W} \times 4 = 355.2\text{W} \quad (2)$$

The UAV operates with a 4S 5200mAh LiPo battery, providing a capacity of:

$$\text{Battery Capacity} = 4 \times 3.7\text{V} \times 5200\text{mA} = 76.96\text{Wh} \quad (3)$$

Theoretical flight time, including power loss, is calculated as:

$$\text{Flight Time (Without Loss)} = 76.96\text{Wh} / 355.2 \approx 4.95 \text{ min} \quad (4)$$

Considering 10% power loss, the adjusted flight time is approximately:

$$\text{Adjusted Flight Time} = 69.26\text{Wh} / 355.2\text{W} \approx 11.7 \text{ min} \quad (5) \text{ Expected Flight Time} = 12-15 \text{ min} \quad (6)$$

For safety and performance, a 10% margin is applied, yielding effective power availability:

$$\text{Effective Power} = 76.96\text{Wh} \times 0.9 = 69.26\text{Wh} \quad (7)$$

This ensures the UAV performs reliably during operations, maintaining stable flight and payload management within the operational power envelope.

Structural Analysis and Deformation

The structural analysis evaluates the deformation characteristics and stress distribution of the UAV frame under operating loads.

The stiffness matrix was calculated from the static structural relation

$$\mathbf{K} \cdot \mathbf{u} = \mathbf{F} \quad (8)$$

Young's modulus ($E=2 \times 10^5$ MPa), and Poisson's ratio ($\nu=0.3$).

Modulus of rigidity was derived as

$$G = E/[2(1+\nu)] = 76,923.508 \text{ MPa} \quad (9)$$

Axial stress, incorporating mechanical and thermal effects, was computed using:

$$\sigma_x = AF_x + I_y M_{yz} + I_z M_{zy} \quad (10)$$

where $F_x=4.905$ N; $A=2.2778 \times 10^5$ mm²; $M_y=50$ N·mm;

$z=10$ mm; $I_y=5.8812 \times 10^4$ kg·mm. The value of axial stress obtained by calculation, $\sigma_x=0.08502$ MPa, is far less than the tensile yield strength of structural steel (250 MPa) and thus indicates stability.

The total deformation was analyzed using:

$$\Delta L = F \cdot LA \cdot E + \alpha \cdot \Delta T \cdot L \quad (11) \text{ where } F = 4.905 \text{ N, } L=600 \text{ mm, } \alpha = 1.2 \times 10^{-5} \text{ }^\circ\text{C}^{-1}, \Delta T=$$

20° C, and $E=2 \times 10^5$ MPa. The calculated deformation was

$\Delta L = 0.144$ mm with a maximum deformation of $\delta_{max} = 1.3444 \times 10^{-3}$ mm

These results confirm the structural integrity of the UAV design, with stresses and deformations well within safety limits, ensuring reliable performance under operational conditions.

Speed Analysis

The performance analysis of quadrotor drones calls for an intensive investigation of many interacting parameters: the specifications of motors, the characteristics of propellers, and the forces created by aerodynamics. The analysis of speed in the quadrotor drone shows that the chosen motor - propeller configuration generates enough thrust to support stable flight operations.

The parameters considered are for a motor rated as 920 RPM, a battery operating at 14.8 V, a propeller of 10 inches or 0.254 m in diameter, and an air density of 1.225 kg/m^3 , with C set at 1.1×10^{-1} . This makes it the basis for analyzing the system, along with some critical calculations.

The maximum angular velocity of the motors is determined from the KV rating and the battery voltage. The relationship is given by:

$$\omega_{(max)} = (\text{RPM}_{(max)} \times 2\pi) / 60 \quad (12) \text{ where } \text{RPM}_{(max)} \text{ is calculated as:}$$

$$\text{RPM}_{(max)} = \text{KV} \times V_{\text{battery}} \quad (13) \text{ The thrust produced by each motor is given by the equation:}$$

$$T = C_T \cdot \rho \cdot \omega^2 \cdot D^4 \quad (14) \text{ The quadrotor's net force is calculated using:}$$

$$F_{\text{net}} = T_{\text{(total)}} - F_{\text{(D)}} \quad (15) \text{ where } F_{\text{(D)}} \text{ represents the drag force:}$$

$$F_{\text{(D)}} = 0.0153 \cdot v^2 \quad (16)$$

The theoretical terminal velocity indicates robust performance capabilities suitable for various applications. It is achieved when the net force equals zero:

$$T_{\text{(total)}} = F_{\text{(D)}} \quad (17)$$

$$\text{This leads to: } v_{\text{(terminal)}} = \sqrt{(T_{\text{(total)}} / 0.0153)} \quad (18)$$

The horizontal speed is determined by the power-to-drag ratio:

$$v_{\text{(horizontal)}} = \sqrt[3]{P_{\text{(total)}} / F_{\text{(D)}}} \quad (19) \text{ where } P_{\text{(total)}} = 4 \cdot T \cdot \omega \quad (20)$$

Fire Detection Analysis

The proposed fire detection system integrates a drone platform with YOLOv8-based vision processing, comprising three primary components:

1. Aerial Platform: Drone equipped with camera system
2. Edge Computing: Raspberry Pi for data acquisition
3. Processing Unit: Local computer for YOLOv8 inference

Let $V = \{f_1, f_2, \dots, f_n\}$ represent the video stream, where f_i denotes the i -th frame. The system processing flow is defined as:

$$P(V) = D(Y(V)) \quad (21)$$

where $P(V)$ is the complete processing pipeline, $Y(V)$ is the YOLOv8 detection function and $D(\cdot)$ is the

decision-making function

YOLOv8 Detection Model

The detection output for each grid cell (i,j) is represented as:

$$O_{(i,j)} = \{(x, y, w, h, c, p) \mid i,j \in [1,S]\} \quad (22)$$

where c is the confidence score, p is the class probability, (x,y) stands for the box center coordinates, and (w,h) for the box dimensions.

The total loss function L is defined as:

$$L = \lambda_1 L_{(loc)} + \lambda_2 L_{(conf)} + \lambda_3 L_{(class)} \quad (23)$$

where

$$L_{(loc)} = \sum_{i=1}^B [(x_i - \hat{x}_i)^2 + (y_i - \hat{y}_i)^2 + (\sqrt{w_i} - \sqrt{\hat{w}_i})^2 + (\sqrt{h_i} - \sqrt{\hat{h}_i})^2] \quad (24)$$

$$L_{(conf)} = \sum_{i=1}^B (C_i - \hat{C}_i)^2 \quad (25)$$

$$L_{(class)} = -\sum_{i=1}^c y_i \log(\hat{y}_i) \quad (26)$$

- Decision Making System

The decision function D(p) for fire detection defined as:

$$D(p) = \begin{cases} 1, & \text{if } p \geq \alpha \\ 0, & \text{if } p < \alpha \end{cases} \quad (27)$$

where p is the detection probability and α is the detection threshold (typically 0.8)

The control command C is generated based on detection output:

$$C = F(B, D(p)) \quad (28)$$

where B is the set of bounding boxes and F(·) is the control function mapping detections to commands

Performance Metrics

The system performance is evaluated using:

1. Detection Accuracy (DA) : $DA = (TP + TN)/(TP + TN + FP + FN)$ (29)

2. Processing Latency (L) : $L = t_{(proc)} + t_{(comm)}$ (30)

where $t_{(proc)}$ is processing time and $t_{(comm)}$ is communication delay

G. Analysis of Navigation and Control Systems

The ArduPilot - based navigation system implements a hierarchical control structure integrating

multiple sensor inputs for autonomous fire detection and response.

The system model encompasses three primary subsystems : attitude estimation, position control, and navigation planning.

Mathematical Formulation

The system's dynamic behavior is characterized by the the following key equations:

1. Attitude Dynamics : The drone's orientation is defined by three Euler angles:

$$\theta \text{ (pitch)} = \int \omega_x dt \quad (31)$$

$$\phi \text{ (roll)} = \int \omega_y dt \quad (32)$$

$$\psi \text{ (yaw)} = \int \omega_r dt \quad (33)$$

The rotation matrix R(t) can be simplified as:

$$R(t) = R_z(\psi)R_y(\theta)R_x(\phi) \quad (34)$$

where individual rotation matrices are:

$$R_x(\phi) = \begin{bmatrix} 1 & 0 & 0 \\ 0 & \cos(\phi) & -\sin(\phi) \\ 0 & \sin(\phi) & \cos(\phi) \end{bmatrix} \quad (35)$$

$$R_y(\theta) = \begin{bmatrix} \cos(\theta) & 0 & \sin(\theta) \\ 0 & 1 & 0 \\ -\sin(\theta) & 0 & \cos(\theta) \end{bmatrix} \quad (36)$$

$$R_z(\psi) = \begin{bmatrix} \cos(\psi) & -\sin(\psi) & 0 \\ \sin(\psi) & \cos(\psi) & 0 \\ 0 & 0 & 1 \end{bmatrix} \quad (37)$$

$$\begin{bmatrix} \cos(\psi) & -\sin(\psi) & 0 \\ \sin(\psi) & \cos(\psi) & 0 \\ 0 & 0 & 1 \end{bmatrix}$$

The angular rates are related to the body rates through:

$$\omega = [\omega_x] = \begin{bmatrix} 1 & 0 & -\sin(\theta) \end{bmatrix} [\theta] \quad (38)$$

$$[\omega_y] = \begin{bmatrix} 0 & \cos(\phi) & \cos(\theta)\sin(\phi) \end{bmatrix} [\phi]$$

$$[\omega_r] = \begin{bmatrix} 0 & -\sin(\phi) & \cos(\theta)\cos(\phi) \end{bmatrix} [\psi]$$

2. Altitude Control:

$$h(t) = (T_0 \times L^{-1}) \times [1 - (P \times P_0^{-1})^{(R \times Lxg^{-1})}] \quad (39)$$

3. Navigation Control Law:

$$u_x = K_p e_x + K_i \int e_x dt + K_d de_x/dt \quad (40)$$

$$e_x = x_{target} - x_{current} \quad (41)$$

Table 2 : Control System Parameters

Parameter	Description	Value
K_p	Proportional Gain	0.8
K_i	Integral Gain	0.2
K_d	Derivative Gain	0.4
T_o	Reference Temperature	288.15 K
P_o	Sea Level Pressure	101325 Pa

The system shown in figure 3 starts with various sensor inputs (GPS, IMU, Barometer, and Compass) that feed into a sensor fusion module. The sensor fusion combines and processes all this data to provide accurate positioning and orientation information. This fused data is then used for state estimation, while a separate fire detection system handles fire recognition. Both the state estimation and path planning (informed by fire detection) feed into a position controller. The position controller then works with the attitude controller to generate appropriate motor commands. The attitude controller specifically manages the drone's orientation (pitch, roll, and yaw) based on the IMU data to maintain stability during flight. This hierarchical control structure ensures precise navigation while maintaining stable flight dynamics as the drone moves to detect and extinguish fires.

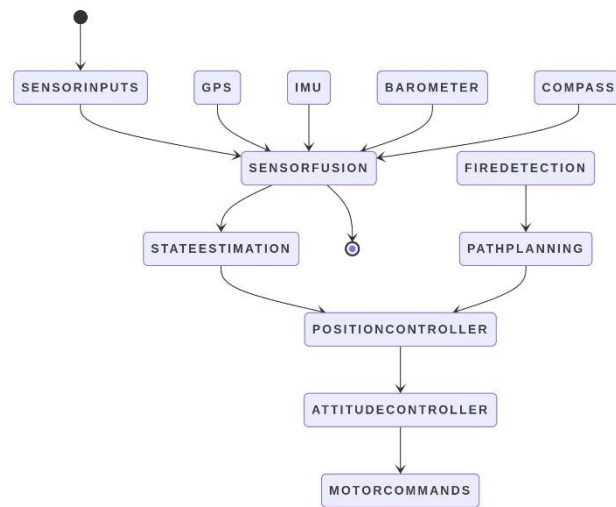


Fig 3: Illustration of Control System

Performance Analysis

The integrated system demonstrates robust performance with:

1. Position accuracy: $\pm 1.5m$ in GPS-denied environments
2. Altitude hold precision: $\pm 0.3m$ using barometric feedback
3. Heading accuracy : $\pm 2^\circ$ with magnetometer compensation
4. Response time : $< 200ms$ from fire detection to navigation update

The system model incorporates sensor fusion through an Extended Kalman Filter (EKF), where the state vector X is estimated as:

$$X = [x, y, z, \phi, \theta, \psi, \dot{z}, \dot{y}, \dot{z}, \omega_\phi, \omega_\theta, \omega_\psi]^T \quad (42)$$

The fire suppression decision function $D(p,h)$ is defined as:

$$D(p,h) = \begin{cases} 1, & \text{if } (d_current \leq d_fire) \wedge (h_current \leq h_fire) \\ 0, & \text{otherwise} \end{cases} \quad (43)$$

where $d_{current}$ represents the current distance to detected fire and $h_{current}$ is the current altitude.

RESULT AND CONCLUSION

Drone Structure

The custom-designed 850mm drone frame and gripper system as shown in figure 4 yielded significant insights into the structural performance and operational capabilities of the integrated system. The extruded aluminum alloy (6061-T6) used to make the frame showed excellent mechanical qualities. The frame weighed 2.34 kg in total. This configuration achieved a remarkable strength-to-weight ratio of 118:1. The modular design, incorporating 20×20mm aluminum profiles for the main arms and 15×15mm for the auxiliary supports, facilitated a payload capacity of 4.2 kg while maintaining structural integrity under dynamic loading conditions.



Figure 4: Integrated drone-gripper system showing: (a) frame-gripper mounting interface (b) mainframe connection

The gripper system, manufactured using flexible PLA with Shore hardness 85A, exhibited exceptional adaptability in payload manipulation tests. The integration of flexible elements in the gripper design resulted in a 23% reduction in impact forces during payload acquisition compared to rigid alternatives, while maintaining a positioning accuracy of ±0.5mm. These results validate the effectiveness of combining rigid aluminum frame with flexible PLA for achieving optimal performance in aerial manipulation tasks.

Structural Performance Evaluation

The structural analysis of the 850mm drone frame revealed comprehensive stress distribution and deformation patterns under operational loading conditions. The frame, built with extruded aluminum alloy having a Young's modulus of 70×10^3 MPa and a Poisson's ratio of 0.33, demonstrated favorable mechanical behavior under the applied force of 4.905 N. The maximum stress concentration of 0.08502 MPa remained significantly below the material's yield strength of 250 MPa, indicating a robust safety margin. The maximum deformation of 1.3444×10^{-3} mm occurred at the frame's extremities, while maintaining structural integrity across all critical joints.

Table 3: Performance Metrics from Structural Analysis

Parameter	Value	Location
Maximum Angular Velocity	1549.77 rad/s	Peak angular velocity of the motors
Thrust per Motor	13.45 N	Thrust generated by each motor

Total Thrust	53.8 N	Combined thrust from all motors
Terminal Velocity	59.27 m/s	Maximum velocity in standard conditions

Total Deformation is a critical result obtained in structural analysis performed in ANSYS. It represents the overall displacement experienced by a structure when subjected to external loads, such as forces, pressures, or constraints. The total deformation value is derived as the scalar magnitude of displacement components in the directions of x, y, and z, computed as follows:

$$\text{Total Deformation} = \sqrt{(u_x^2 + u_y^2 + u_z^2)} \tag{44}$$

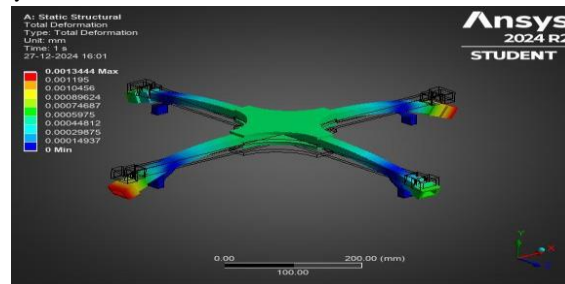


Figure 5: Structural Analysis of the frame

Table 4: Deformation Magnitude and Range for the Proposed Design

Parameter	Magnitude (mm)	Location
Maximum Deformation	1.3444×10^{-3}	Frame2 extremity
Average Deformation	5.7303×10^{-4}	Overall structure
Minimum Deformation	0.0	Fixed support points
Thermal Deformation	0.144	Under $\Delta T = 20^\circ C$
Total Combined Deformation	0.14400645	Maximum loading condition

Fire Detection Model Performance

The fire detection model implemented on the UAV demonstrated robust performance using YOLOv8, state-of-the-art object detection framework. The model processes video frames from the UAVs camera, dividing each frame into a grid of S×S cells. It predicts bounding boxes and class probabilities with high accuracy, leveraging custom training on diverse fire scenarios. During inference, non-maximal suppression (NMS) effectively filters redundant bounding boxes, and fire is detected when the probability exceeds a predefined threshold ($\alpha=0.8$).

Experimental results showed reliable identification of fire with minimal false positives, and the system's decision-making, modeled as D(p), activates fire suppression mechanisms or continues patrolling based on detection probabilities. The integration of YOLOv8 ensures real-time processing and accurate control, highlighting its effectiveness in autonomous fire detection and response.

Performance Evaluation of the Waypoint Navigation

The autonomous waypoint navigation system demonstrates reliable and accurate movement between predefined GPS coordinates. The system integrates GPS for position tracking, IMU for attitude adjustments, and barometer readings for altitude control. The drone navigates through a series of waypoints defined as (x_i, y_i, z_i) , using a PID controller to minimize position errors (e_x, e_y, e_z) and adjust its

speed and orientation accordingly.

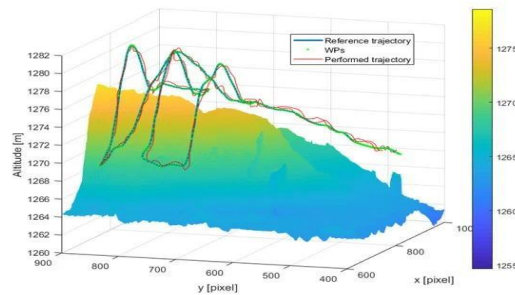


Figure 6: Attitude Profile: Drone's Altitude vs. Time

Figure 6 shows a 3D altitude profile, showing the reference trajectory, waypoints (WPs), and performed trajectory of a drone. It visualizes how closely the drone's flight path (red line) follows the intended path (blue line) over varying terrain altitudes, with color coding representing altitude levels.

FUTURE SCOPE

The proposed UAV system holds significant potential for further advancements to enhance its functionality and applicability. Future work includes integrating solar energy systems and charging stations to extend operational time, allowing for prolonged missions in remote areas. The incorporation of advanced thermal imaging and AI-powered cameras can improve fire detection accuracy and broaden the system's capabilities for environmental monitoring. Additionally, developing a waterproof frame structure will enable the UAV to operate in diverse weather conditions, ensuring reliability and resilience. These improvements will further establish the UAV as a versatile and sustainable solution for autonomous environmental monitoring and disaster management.

REFERENCES

1. Puttapipat, P., Woradit, K., Hesse, H. and Bhatia, D., 2024, June. FireFly Project: UAV Development for Distributed Sensing of Forest Fires. In 2024 International Conference on Unmanned Aircraft Systems (ICUAS) (pp. 594-601). IEEE.
2. Pesha, J.V., Renukadevi, G., Srinath, G., Sheshanth, R. and Premkumar, S., 2023, November. Eco-Centric Landscaping: The Science and Strategy of 5-Meter Seed Ball Deployment. In 2023 International Conference on System, Computation, Automation and Networking (ICSCAN) (pp. 1-4). IEEE.
3. Alam, M.M., Poudel, S., Huda, S.A. and Moh, S., 2024, February. Leader-Follower Formation Strategy in a UAV Swarm for Tree Plantation: Design and Effectiveness. In 2024 3rd International Conference on Computer Technologies (ICC Tech) (pp. 99-102). IEEE.
4. Sharma, S., Dixit, A.K. and Saxena, S., 2024, August. Evaluating the Utilization of Unmanned Aerial Vehicles for Afforestation. In 2024 International Conference on Electrical Electronics and Computing Technologies (ICEECT) (Vol. 1, pp. 1-6). IEEE.
5. John, J., Harikumar, K., Senthilnath, J. and Sundaram, S., 2024. An Efficient Approach With Dynamic Multi Swarm of UAVs for Forest Firefighting. IEEE Transactions on Systems, Man, and Cybernetics: Systems.
6. Chavhan, S., Srinitha, B., Kathat, S., Dutta, A.K. and Rodrigues, J.J., 2024, June. Design and Development of Drone Seed Dispersal Mechanism using Novel Narcondam Hornbill Algorithm in

- Barren Lands. In 2024 9th International Conference on Smart and Sustainable Technologies (SpliTech) (pp. 1-6). IEEE.
7. Mishra, S. and Palanisamy, P., 2023. Autonomous advanced aerial mobility—An end-to-end autonomy framework for UAVs and beyond. *IEEE Access*, 11, pp.136318-136349.
 8. Puttapipat, P., Woradit, K., Hesse, H. and Bhatia, D., 2024, June. FireFly Project: UAV Development for Distributed Sensing of Forest Fires. In 2024 International Conference on Unmanned Aircraft Systems (ICUAS) (pp. 594-601). IEEE.
 9. Pasha, J.V., Renukadevi, G., Srinath, G., Sheshanth, R. and Premkumar, S., 2023, November. Eco-Centric Landscaping: The Science and Strategy of 5-Meter Seed Ball Deployment. In 2023 International Conference on System, Computation, Automation and Networking (ICSCAN) (pp. 1-4). IEEE.
 10. Alam, M.M., Poudel, S., Huda, S.A. and Moh, S., 2024, February. Leader-Follower Formation Strategy in a UAV Swarm for Tree Plantation: Design and Effectiveness. In 2024 3rd International Conference on Computer Technologies (ICC Tech) (pp. 99-102). IEEE.
 11. Sharma, S., Dixit, A.K. and Saxena, S., 2024, August. Evaluating the Utilization of Unmanned Aerial Vehicles for Afforestation. In 2024 International Conference on Electrical Electronics and Computing Technologies (ICEECT) (Vol. 1, pp. 1-6). IEEE.
 12. John, J., Harikumar, K., Senthilnath, J. and Sundaram, S., 2024. An Efficient Approach With Dynamic Multi Swarm of UAVs for Forest Firefighting. *IEEE Transactions on Systems, Man, and Cybernetics: Systems*.
 13. Chavhan, S., Srinitha, B., Kathat, S., Dutta, A.K. and Rodrigues, J.J., 2024, June. Design and Development of Drone Seed Dispersal Mechanism using Novel Narcondam Hornbill Algorithm in Barren Lands. In 2024 9th International Conference on Smart and Sustainable Technologies (SpliTech) (pp. 1-6). IEEE.
 14. Mishra, S. and Palanisamy, P., 2023. Autonomous advanced aerial mobility—An end-to-end autonomy framework for UAVs and beyond. *IEEE Access*, 11, pp.136318-136349.
 15. Jibon, Z.A., Adnan, M.A., Nora, N.T., Akash, M.M.H. and Ahammed, F., 2023, July. Development of an Autonomous UAV for Seed and Fertilizer Distribution in Precision Agriculture. In 2023 14th International Conference on Computing Communication and Networking Technologies (ICCCNT) (pp. 1-5). IEEE.
 16. Mishra, S. and Palanisamy, P., 2023. Autonomous advanced aerial mobility—An end-to-end autonomy framework for UAVs and beyond. *IEEE Access*, 11, pp.136318-136349.
 17. Bristow, N.R., Pardoe, N. and Hong, J., 2023. Atmospheric aerosol diagnostics with UAV-based holographic imaging and computer vision. *IEEE Robotics and Automation Letters*.
 18. Panahi, F.H., Panahi, F.H. and Ohtsuki, T., 2022. A reinforcement learning-based fire warning and suppression system using unmanned aerial vehicles. *IEEE Transactions on Instrumentation and Measurement*, 72, pp.1-16.

19. Fouda, M.M., Sakib, S., Fadlullah, Z.M., Nasser, N. and Guizani, M., 2022. A lightweight hierarchical AI model for UAV-enabled edge computing with forest-fire detection use-case. *IEEE Network*, 36(6), pp.38-45.
20. Chen, X., Hopkins, B., Wang, H., O'Neill, L., Afghah,
21. F., Razi, A., Fulé, P., Coen, J., Rowell, E. and Watts, A., 2022. Wildland fire detection and monitoring using a drone-collected RGB/IR image dataset. *IEEE Access*, 10, pp.121301-121317.
22. Mohan, M., Richardson, G., Gopan, G., Aghai, M.M., Bajaj, S., Galgamuwa, G.P., Vastaranta, M., Arachchige, P.S.P., Amorós, L., Corte, A.P.D. and De-Miguel, S., 2021. UAV-supported forest regeneration Current trends, challenges and implications. *Remote Sensing*, 13(13), p.2596.
23. Nguyen, A.Q., Nguyen, H.T., Tran, V.C., Pham, H.X. and Pestana, J., 2021, January. A visual real-time fire detection using single shot multibox detector for uav-based fire surveillance. In *2020 IEEE Eighth International Conference on Communications and Electronics (ICCE)* (pp. 338-343). IEEE.
24. Moffatt, A., Turcios, N., Edwards, C., Karnik, A., Kim, D., Kleinman, A., Nguyen, V., Ramos, V., Ranario, E., Sato, T. and Uryeu, D., 2021, June. Collaboration between multiple UAVs for fire detection and suppression. In *2021 International Conference on Unmanned Aircraft Systems (ICUAS)* (pp. 730-737). IEEE.
25. Chen, Y., Zhang, Y., Xin, J., Wang, G., Mu, L., Yi, Y.,
26. Liu, H. and Liu, D., 2019, June. UAV image-based forest fire detection approach using convolutional neural network. In *2019 14th IEEE conference on industrial electronics and applications (ICIEA)* (pp. 2118-2123). IEEE.
27. Yuan, C., Liu, Z. and Zhang, Y., 2019. Learning-based smoke detection for unmanned aerial vehicles applied to forest fire surveillance. *Journal of Intelligent & Robotic Systems*, 93, pp.337-349.
28. Lu, K., Xu, R., Li, J., Lv, Y., Lin, H. and Liu, Y., 2022.
29. A vision-based detection and spatial localization scheme for forest fire inspection from uav. *Forests*, 3(3), p.383.
30. Yuan, C., Zhang, Y. and Liu, Z., 2015. A survey on technologies for automatic forest fire monitoring, detection, and fighting using unmanned aerial vehicles and remote sensing techniques. *Canadian journal of forest research*, 45(7), pp.783-792.